UNIVERSIDADE FEDERAL DA PARAÍBA

CENTRO DE CIÊNCIAS DA SAÚDE

PROGRAMA DE PÓS-GRADUAÇÃO EM ODONTOLOGIA

ANÁLISE QUANTITATIVA DA INFILTRAÇÃO DE QUINOLINA EM LESÕES CARIOSAS NATURAIS PROXIMAIS DE ESMALTE

Camila Santos de Mattos Brito

2014

CAMILA SANTOS DE MATTOS BRITO

ANÁLISE QUANTITATIVA DA INFILTRAÇÃO DE QUINOLINA EM LESÕES CARIOSAS NATURAIS PROXIMAIS DE ESMALTE

Dissertação apresentada ao Programa de Pós-Graduação em Odontologia, da Universidade Federal da Paraíba, como parte dos requisitos para obtenção do título de Mestre em Odontologia – Área de Concentração em Odontologia Preventiva e Infantil.

Orientador: Prof. Dr. Frederico Barbosa de Sousa

João Pessoa

2014

CAMILA SANTOS DE MATTOS BRITO

ANÁLISE QUANTITATIVA DA INFILTRAÇÃO DE QUINOLINA EM LESÕES CARIOSAS NATURAIS PROXIMAIS DE ESMALTE

Banca Examinadora

Prof. Dr. Frederico Barbosa de Sousa

Orientador - UFPB

Prof. Drª. Ana Maria Barros Chaves Pereira

Examinador - UFPB

Prof. Dr. Aline de Almeida Neves

Examinador - UFRJ

DEDICATÓRIA

Dedico com todo o meu amor aos meus pais, que sempre acompanharam e incentivaram meus passos na docência, desde as aulas de origami, as aulas de inglês e reforço, e agora rumo ao ensino superior. Tudo que faço, faço pensando em deixá-los orgulhosos.

AGRADECIMENTOS

A Deus, como não poderia deixar de ser, por tornar tudo possível. Por todas as oportunidades que tive, e por fornecer toda a calma e confiança de que, de uma forma ou de outra, tudo daria certo no final.

Aos Santos e aos Mattos Brito, que sem exagero nenhum, posso dizer que são os melhores do mundo. Sinto-me até um pouco culpada de ter concentrado todas as pessoas especiais em uma família só, mas suspeito que haja outras pessoas quase tão legais quanto em outras famílias por aí.

Em especial aos meus avós maternos e paternos, a quem também dedico este trabalho. Sou privilegiada de tê-los por perto, mesmo morando longe, mas sempre presentes em todas as conquistas. Aqui vai mais uma etapa concluída, e agradeço todo o apoio e incentivo de hoje e de sempre.

Ao orientador Frederico Barbosa, que acredito que nem imagina o quanto sou realmente grata por toda a paciência, aprendizados, experiências e acima de tudo, exemplo do tipo de profissional que quero me tornar. Sua competência e dedicação são inspiradoras.

Aos companheiros diários de LAMIB, Kássia, Danilo, Fernanda, Patrícia, Lúcia, Emanuella, Plínio, Adami, Cinthia e Maria Luisa, com quem tive a convivência mais intensa dos últimos dois anos, e os únicos que realmente compreendem a dimensão que teve esta pesquisa em minha vida.

A Yuri Gonzaga, que sempre foi a pessoa certa na hora certa, me fazendo feliz todos os dias. A companhia mais agradável, mesmo nos momentos mais atribulados. Sempre solícito e não medindo esforços para ajudar. Além de ser responsável pelo desenvolvimento dos softwares que salvaram nossas vidas.

Aos meus colegas do mestrado, que passaram por todos os sufocos juntos comigo. Desde a espera do resultado na seleção, até essa reta final. Alguns já conhecidos e queridos, outros que me conquistaram no decorrer destes dois anos. Vocês tornaram tudo mais leve e divertido.

Agradeço especialmente as colegas e amigas Julyana e Laudenice, que foram de grande ajuda e possibilitaram a realização desta pesquisa, através da coleta de dentes.

E que venham as próximas etapas, pois sei que poderei contar com vocês.

“Aqui chegamos, enfim
A um ponto sem regresso
Ao começo do fim
De um longo e lento processo
Que se apressa a cada ano
Como um progresso insano
Que marcha pro retrocesso
E é só o começo

Estranhos dias vivemos
Dias de eventos extremos
E de excessos em excesso
Mas se com tudo que vemos
Os olhos viram do avesso
Outros eventos veremos
Outros extremos virão
Prepare seu coração
Que isso é só o começo”

Lenine

RESUMO

A imersão em quinolina de lesões naturais de cárie em esmalte tem sido importante para determinar o tamanho da lesão e áreas com diferentes tamanhos de poros. No entanto, dados volumétricos quantitativos resultantes da infiltração desta substância não estão disponíveis na literatura. Sendo assim, o presente trabalho objetivou apresentar os primeiros dados quantitativos volumétricos do infiltrado por quinolina (na maioria das amostras < 50 % do volume de poros foram infiltrados) em camadas histológicas (incluindo zona escura) de cortes por desgaste de lesões cariosas naturais em esmalte (n = 20). Além disto, verificou-se que um parâmetro relacionado à permeabilidade previu 60 % da variância da infiltração volumétrica. A distância da superfície do esmalte original foi inversamente relacionada com o volume infiltrado. Na maioria das lesões, a zona translúcida não foi o *front* da lesão. Mapeamento em 2D em tempo real de processos de transporte após a imersão em quinolina, através de microscopia de luz polarizada, revelou primeiramente um fluxo de água para o exterior e uma conseguinte penetração por quinolina, ambos seguindo a trajetória dos prismas paralelamente ao eixo principal dos cortes por desgaste. Novos eventos da natureza dos processos de transporte em cortes por desgaste aqui relatados podem ser explorados para melhorar a eficiência de ambos os agentes remineralizantes e infiltrantes de resina para tratamento de lesões cariosas.

Palavras-chave: esmalte, cárie dental, histologia, permeabilidade, zona escura.

ABSTRACT

Immersion of natural enamel caries (NEC) in quinoline has been important for determining lesion size and mapping areas with different pore sizes, but quantitative volumetric data of the infiltration are not available. Here we provide first quantitative volumetric data of the volume infiltrated by quinoline (mostly < 50% of pore volume were infiltrated) in histological layers (including dark zone) of ground sections of NEC lesions (n = 20) and report that a parameter related to permeability predicted 60% of the variance of the volumetric infiltration. Distance from the original enamel surface was inversely related to the infiltrated volume. In most lesions the translucent zone was not the lesion front. Real-time 2D mapping of transport processes after immersion in quinoline revealed an early outward water flow and a late inward quinoline penetration, both following prisms paths parallel to the main axis of ground sections. New events of the nature of transport processes in ground sections of NEC lesions reported here can be explored to improve efficiency of both remineralizing agents and resin infiltrants for treatment of NEC.

Keywords: enamel; dental caries; histology; permeability; dark zone

SUMÁRIO

1. INTRODUÇÃO

O esmalte, tecido que recobre a coroa do elemento dental, é a estrutura mais mineralizada do corpo humano, apresentando volume mineral próximo a 90%. A porcentagem remanescente é constituída por matéria orgânica e água[10,34,23].

Seu componente mineral encontra-se na forma de cristais de apatita e são compactados em colunas definidas como prismas. Esse arranjo dá origem a uma estrutura porosa, estando os poros localizados entre os cristais[39].

O principal componente inorgânico do esmalte é o fosfato de cálcio na forma de cristais de hidroxiapatita ($Ca_{10}(PO_4)_6OH_2$), porém outros constituintes inorgânicos, se presentes no período de formação do esmalte dental, podem ser incorporados à estrutura da apatita. Esta contém uma quantidade considerável de grupos carbonato, que substituem a hidroxila (OH^-) ou o fosfato tetraédrico (PO_4). Pode-se encontrar ainda, em concentrações mais baixas e variáveis, outros constituintes tais como potássio, cloreto, carbonato, sódio, magnésio entre outros[15,22]. A composição exata varia entre dentes, em diferentes partes do mesmo dente e até mesmo entre o centro e a periferia do mesmo prisma. Análises químicas e os dados cristalográficos comprovam a não homogeneidade do esmalte[13].

Diversos estudos, através de análises bioquímicas, têm proposto uma fórmula para a célula unitária da apatita do esmalte humano normal[12,3,15]. Elliott[16] propôs para a apatita a fórmula $Ca_{8.856}Mg_{0.088}Na_{0.292}K_{0.010}(PO4)_{5.312}(HPO4)_{0.280}(CO3)_{0.407}(OH)_{0.702}Cl_{0.078}(CO3)_{0.050}$, obtendo uma densidade de 2.99 g cm^{-3} para a mesma. Baseado nos dados de Elliot[15], Sousa, Vianna e Santos-Magalhães[34] encontraram para o esmalte dental maduro, 92% de volume mineral e 2% e 6% de volumes de matéria orgânica e água, ajustando, pela primeira vez, os valores destes três componentes em 100%[15,34].

Em relação à composição orgânica, esta é dada por proteínas, principalmente amelogenina e enamelina, e por uma pequena quantidade de

lipídeos[17]. A matéria orgânica situa-se no interior dos poros do esmalte, rodeando a hidroxiapatita[32,22].

O terceiro componente do esmalte é a água. Esta se encontra sob duas formas[10]: água firmemente aderida, que é incorporada como uma camada de hidratação ao redor dos cristais do mineral e está ionizada em OH^- e H^+ (formando íons HPO_4^{2-}). Já a água adsorvida, fracamente aderida ou livre, encontra-se no interior dos poros e pode ser removida com mais facilidade[6,2,15]. Para He[24] devido a dificuldades técnicas, a quantificação da água firmemente e fracamente aderida não tem sido realizada com precisão[24].

Embora seja apenas uma pequena parte do esmalte, a água desempenha um papel importante na função, pois mudanças em sua quantidade alteram significantemente as propriedades mecânicas do tecido[29].

Uma das contribuições mais influentes no campo da patologia da cárie veio a partir da interpretação da birrefringência do esmalte cariado sob microscopia de luz polarizada (MLP) e através da radiomicrografia[9,31,18]. Tanto em lesões de dentes permanentes como em decíduos, diferentes zonas com conteúdo mineral variável foram distinguidas utilizando microscopia de luz polarizada[9,33].

A birrefringência de esmalte vem do mineral (birrefringência intrínseca, com o sinal negativo) e dos volumes não-minerais (birrefringência de forma, com sinal positivo), de modo que a imagem de esmalte em MLP (a birrefringência observada) é um resultado da soma destes dois tipos de birrefringência[34]. Na década de 1950, Darling[8] propôs uma abordagem matemática para interpretar birrefringência observada do esmalte (BR_{obs}) que lhe permitiu obter informações estruturais em pontos histológicos. Esta abordagem é baseada na aplicação de um procedimento duplo para interpretar birrefringência do esmalte[8], isto é:

(i) a utilização de meios de imersão com índices de refração e tamanhos moleculares diferentes (ar, água e quinolina) em secções por desgaste da mesma lesão, e

(ii) a aplicação de uma abordagem matemática, análise qualitativa dos tamanhos e volume dos poros[9].

A análise de Darling[8] se tornou extremamente popular. Nesta análise, aplicou-se o pressuposto de que os poros do esmalte são preenchidos por um único componente (e um único índice de refração), o meio de imersão (modelo clássico do índice de refração da fase não mineral, neste caso, sendo representado por n_2)[8]. Esse modelo foi usado para adaptar a equação de Wiener[38] para a birrefringência de forma (relacionada ao volume não mineral) do esmalte. Esta clássica equação foi formulada para materiais heterogêneos compostos por diferentes fases, cada uma com seu próprio índice de refração (n) e volume.

De acordo com a abordagem matemática de Darling[8], considerando um mesmo meio de imersão, qualquer alteração na birrefringência é interpretada como alteração no volume mineral, uma vez que só são considerados dois volumes no esmalte (volume mineral, com índice de refração n_1, e volume não mineral, com índice de refração n_2)[8]. Apesar de, em torno da época desta publicação já ser conhecido que os poros do esmalte possuem matéria orgânica e que sua água não é completamente removida à temperatura ambiente[1], esse modelo teve popularidade por não ter sido proposta nenhuma melhor aproximação para interpretar a birrefringência do esmalte. A grande quantidade de informação que a imagem do esmalte em microscopia de luz polarizada proporcionava era bastante atrativa para os pesquisadores. Como interpretação, só havia a opção do modelo de Darling[8].

Em geral, as experiências de Darling incluíram imersão em ar e em soluções com baixo (1,33) e elevado (1,62) índices de refração, utilizando tanto baixo e alto tamanho molecular em soluções, obtendo-se pelo menos cinco meios de imersão em uma única lesão[7]. De acordo com seu modelo matemático, o volume de poros no esmalte era estimado com base no sinal da birrefringência observada (soma das birrefringências intrínseca e de forma) em determinado meio de imersão. Os poros grandes eram aqueles infiltrados por quinolina (moléculas grandes), e os poros pequenos aqueles não infiltrados. A interpretação de grande ou pequeno era baseada na ocorrência ou não de redução da birrefringência de forma (redução da diferença n1 – n2) em comparação com que era observado com imersão em ar/água: com redução [resultado de (1,62 – 1,62)

< (1,62-1,33)], se interpretava que os poros eram grandes; sem redução, se interpretava que os poros eram pequenos demais para que a quinolina infiltrasse.

Desta forma, as zonas diferentes em tamanhos de poro e volumes de cárie de esmalte foram descritos: camada superficial, corpo da lesão, zona escura e zona translúcida. É bem conhecido, no entanto, que tais características não são universais, de modo que muitas lesões podem não apresentar as zonas escura e translúcida[33], e ainda a camada superficial[11,28,30,36].

Estas zonas surgem a partir de diferenças no volume de poros do esmalte afetado durante a progressão da cárie. O corpo da lesão tem um volume de cerca de 5-25% de poros, enquanto que a zona escura e a zona translúcida têm um volume de poros entre 1% e 4%[5].

A zona translúcida pode variar de 5 a 100 µm de largura, e nela encontra-se a primeira alteração cariosa visível no esmalte, correspondendo a uma perda mineral de cerca de 1-2%, composta por um pequeno número de poros relativamente grandes. Interpretações iniciais sugeriram que a primeira etapa a acontecer é a remoção de proteínas, seguida de perda de íons inorgânicos. Embora perda de mineral tenha sido mostrada, a perda de material orgânico não foi demonstrada de forma convincente. Muita desta perda inicial também pareceu derivar a partir das regiões interprismática e intercristalinas, devido, em parte, a um fluxo facilitado de íons através destas regiões[7,4,16].

A interpretação de Darling[8] dá suporte matemático para o evento de des e remineralização e para o estabelecimento dos limites da lesão cariosa de esmalte e como o esmalte cariado é contrastado do esmalte normal. Isto tem ampla repercussão em estudos laboratoriais e de campo epidemiológicos, envolvendo patologia, diagnóstico, prevenção e tratamento.

Recentemente, uma nova abordagem matemática foi proposta para interpretar a BR_{obs} do esmalte, em que os volumes de matéria orgânica e de dois tipos de água livre são considerados. Este modelo permitiu obter dados quantitativos dos volumes mineral, de água e matéria orgânica em lesões cariosas[35,27], abrindo novas perspectivas na patologia da cárie de esmalte. De particular interesse neste trabalho, é a zona translúcida.

Considerada como o “front” da lesão pela interpretação de Darling[8], e sendo confirmada posteriormente com dados quantitativos de volume mineral por Hallsworth, Weatherell e Robinson[21], a zona translúcida foi descrita numa localização muito aquém do “front” da lesão natural de esmalte[27]. Este relato abre um questionamento sobre os limites da lesão, que podem estar sendo extremamente subestimados. Uma vez que a zona de BR_{obs} positiva em água (delimitada pela zona translúcida) é relacionada com esmalte opaco, e este é comumente usado como critério para determinar os limites da lesão cariosa de esmalte, a possibilidade da zona translúcida não ser o “front” da lesão coloca em questão um volume gigantesco de dados sobre lesão cariosa do esmalte, merecendo atenção de mais estudos.

Não há dados na literatura sobre o volume de quinolina infiltrado na zona translúcida. Esta é uma outra lacuna que a interpretação da birrefringência do esmalte de Sousa, Vianna e Santos-Magalhães[34] pode ajudar a preencher. Somado a isto, as características qualitativas do esmalte normal ao microscópio de luz polarizada em certos meios de imersão está bem descrita na literatura[7,37,1,19,20,25,14,34], servindo de parâmetro para validar as análises quantitativas. Assim, faz-se jus a uma investigação do volume de quinolina infiltrado na zona translúcida e se esta zona realmente pode ser interpretada como o “front” da lesão.

2. CAPÍTULO 1

O manuscrito a seguir foi submetido para publicação no periódico Acta Biomaterialia e encontra-se em análise.

Natural Enamel Caries in Quinoline: pattern of infiltration

Camila Brito [1]

Kássia Regina [1]

Frederico Barbosa de Sousa[1,2,3*]

[1] Master program in Dentistry, Health Sciences Center, Federal University of Paraiba, Cidade Universitária, 58051-900, João Pessoa, Paraiba, Brazil.

[2] Laboratory of Microscopy and Biological Image, Health Sciences Center, Federal University of Paraiba, Cidade Universitária, 58051-900, João Pessoa, Paraiba, Brazil.

[3] Department of Morphology, Health Science Center, Federal University of Paraiba, Cidade Universitária, 58051-900, João Pessoa, Paraiba, Brazil

***Corresponding author:**

Frederico Barbosa de Sousa

Departamento de Morfologia, Centro de Ciências da Saúde, Universidade Federal da Paraíba, Cidade Universitária, S/N, CEP 58051-900, João Pessoa, Paraíba, Brazil

Tel: +55-83-3216-7254; Fax: +55-83-3216-7094; E-mail: fredericosousa@hotmail.com

Abstract

Immersion of natural enamel caries (NEC) in quinoline and observed in polarized light microscopy has been important for determining lesion size and mapping areas with different pore sizes, but quantitative volumetric data of infiltration are not available. The present study provides first quantitative volumetric data of the volume infiltrated by quinoline (mostly < 50% of pore volume were infiltrated) in histological layers (including dark zone) of ground sections of NEC lesions (n = 20). Moreover, it is reported that a parameter related to permeability predicted 60% of the variance of the volumetric infiltration. Distance from the original enamel surface was inversely related to the infiltrated volume of quinoline. In most lesions the translucent zone was not the lesion front. Real-time 2D mapping of transport processes after immersion in quinoline revealed an early outward water flow and a late inward quinoline penetration, both following prisms paths parallel to the main axis of ground sections. New events on the nature of transport processes in ground sections of NEC lesions reported here can be explored to improve efficiency of both remineralizing agents and resin infiltrants for treatment of NEC.

Keywords: enamel; dental caries; histology; permeability; dark zone

1. Introduction

Variations in the apparent permeability of carious enamel in histological ground sections have long called attention of the scientific community, specially regarding the different histological zones seen in carious enamel when a given material is used as immersion medium [1]. The advent of radiographic techniques with microscopic resolution have also brought up that variations in mineral densities existed [2]. The most influential contributions came from studies with polarizing microscopy combined with the mathematical model proposed by Darling to interpret optical birefringence of enamel [3, 4]. Among the histological zone, a particular feature has called the most attention: a dark zone seen when carious enamel was immersed in an oil medium called quinoline. In the early 60's, it was reported that the relative penetration through the pores of the dark zone was inversely proportional to the molecular size of a wide range of liquids used to imbibe ground sections and that infiltrated into other zones of the same lesions [5, 6]. It was concluded then that the smaller pores in the dark zone resulted from remineralization, and since then, the most influential literature on the histopathology of enamel caries has been based on that assumption[7, 8].

In those studies, enamel was first analyzed after water imbibition, then it was dried and eventually immersed in other liquids. The results obtained from these studies were based on a number of assumptions: (i) all liquids are able to infiltrate dry enamel at reasonably same rate; (ii) all pores are mostly filled only with air (samples have to be dried before they are imbibed in other liquids than water) just before infiltration of the test liquids; and (iii) the dark zone is located in a region which birefringence (under water immersion) is similar to that of normal enamel; and (iv) distances from the initial location of the test liquids (at its start location all around the ground section) to the pores at the various zones of enamel caries start point are reasonably the same [4]. With time new evidence emerged indicating that rehydration of dried (at room temperature)

enamel takes longer than water loss during dehydration of wet enamel, suggesting that drying could lead to conformation changes of the organic matter and this could reduce the diffusion rate of water [9]. It was also shown that concentrated salt solutions could diffuse very slowly, requiring a long time (months) to result in a slight penetration into the pores of normal enamel [10]. Recently, the first quantitative volumetric data on the infiltration of liquid with varying refractive indexes in developing (hypomineralized) enamel provided evidence that diffusion rate is inversely proportional to pore volume [11]. In this way, studies on the infiltration of dark zone have probably neglected the possible variations in the diffusion rates of the different liquids tested and the effect of organic matter (morphologically changed after air drying) involved in it [4, 5, 6]. There is evidence that removal of organic matter with solvents enhances infiltration of quinoline and reduces the size of the dark zone [12], suggesting that the dark zone may not be a result of remineralization. In addition, dark zone is not a universal feature of natural enamel caries (NEC) [13], and it has been shown, in figures published by the same author, that proposed it was located in a relatively normal enamel [4], to be partially located at the most demineralized histological zone of enamel caries (body of the lesion), in a frank contradiction with the most widely accepted description.

A translucent zone is another important histological feature of enamel caries after quinoline imbibition, as it was first suggested to represent the deepest zone (the front) of demineralization in the enamel lesion [4]. There is conflicting evidence that the translucent zone actually represents the front of the lesion [14, 15]. The conflicting evidences on the features of histological of NEC in quinoline, linking permeability only with mineral content, might be a result of the lack of spatially resolved quantitative volumetric data and mechanics of infiltration in ground sections of enamel. The later information have been used to provide new insights into the infiltration of liquids in NEC and a parameter (ratio between squared water volume by non-mineral volume) has been shown as a reasonable good predictor (predicting 50% of variance) of the infiltration. More importantly, information on flow mechanics of the liquids during infiltration

has shown that the distance to be traveled by the liquid and air displacement in the pores during infiltration are major factors that need to be take into account to interpret the nature of the diffusion process in NEC [16]. Studying the infiltration of quinoline is important to further understand the nature of viscous liquids, and resin infiltrants used to arrest NEC are viscous liquids (more than watery liquids), and to validate the size of NEC lesions.

Our previous report [16] indicated that prediction of infiltration could be strengthened with liquids with viscosity higher than that of salt solutions with refractive indexes 1.4-1.47. The aim of this study was thus to test this hypothesis using quinoline. We also tested the hypothesis that distance from the start location of penetration is a factor in the infiltration of NEC lesions by quinoline.

2. Materials and methods

2.1 Samples

Twenty human permanent erupted teeth (third molars and premolars), extracted for clinical health reasons, presenting approximal NEC lesions were collected from volunteers. This study was approv by the Ethical Committee on Human Research of the Health Sciences Center of the Federal University of Paraiba (Brazil). From those teeth, 30 approximal NEC lesions were scored by two calibrated examiners (intra-examiners reliability kappa index of 0.739 and 0.856; inter-examiner kappa index of 0.812) regarding lesion activity and according to the to the ICDAS system [17]. All lesions were examined under stereomicroscopy after removal of organic cover with 1% sodium hypochlorite for 30 seconds followed by air drying with compressed air for 10 seconds. A total of 20 inactive noncavitated approximal NEC lesions were selected for this study. They were cut with diamond discs mounted in low-speed handpieces motors under water irrigation, and then ground sections were prepared (using a lapping jig and sandpaper with

different granulations) with final thickness between 50 and 90 μm. All ground sections were kept in a 0.02 % sodium azide solution before infiltration with air and quinoline.

Final sample thickness was obtained after immersion in quinoline. The sample was then cut using a razor blade under the stereomicroscope, as close as possible to the transversal (maximum distance of 100 μm) and following prisms' paths. After that, sections were positioned edge-on in a transmitted light polarizing microscope equipped with a 20X objective (resolution of 0.7 μm) and digital photomicrograhs were taken in order to perform measurements of thickness with the aid of an image analysis software (ImageJ, NIH, USA).

2.1 Quantification of mineral volume

Quantification of mineral volume (V_1) was performed using the Angmar equation [18], based on a mineral density of hydroxiapatite 2.99 gcm^{-3} [19], as recently described [16]. The non-mineral volume (V_2), the pore volume, was calculated by $1 – V_1$.

In each sample, a transversal line (from the enamel surface to the enamel-dentin junction) was drawn across the NEC lesion and histological points (area of 15 x 15 μm), at 20 μm interval along the transversal, were selected for quantitative measurements of all parameters described in this study. A total of 1124 points comprised the final sample.

All histological points from the enamel surface up to the translucent zone (the later included) comprised what we called the Outer Part of the Enamel Layer. The remaining points, then on to the EDJ, made up the Inner Part of the Enamel Layer.

2.3 Quantification of water and organic volumes and the water more easily available for diffusion (permeability)

For the interpretation of observed birefringence (BR_{obs}) in water, the approach of Sousa et al. [20] was used in order to quantify water (α) and organic (β) volumes (the two constituents of V_2). This procedure has been minutely described in many earlier reports [4, 21, 11]. A custom-made software was used to perform those calculations. It is available on the internet (http://hotfile.com/dl/204330734/6099675/EBI-0.1.jar.html) for free use. Afterwards, we calculated the water more easily available for diffusion (α_d, which we call a permeability parameter) by [21]:

$$\alpha_d = \frac{\alpha^2}{\alpha + \beta} \cdot 100 \quad (1)$$

This equation is the product of α by $\alpha/(100\text{-}V_1)$, standing for the effective pore size and the inverse of pore viscosity, respectively.

2.4 Quantification of quinoline infiltration

After measuring BR_{obs} in water, each sample was dried at room temperature (25º C and 50% of relative humidity) for 48 hs and then immersed in quinoline for 24h.

One of the restrictions in the study of NEC lesions is that, after drying, those lesions become opaque (no birefringence), and therefore loosely bound water (α_2) cannot be directly measured. It is relevant to quantify how much air (which replaces α_2 after drying) was replaced by the infiltrating material and whether it replaced or not part of firmly bound water (α_1) found in

enamel pores after drying. Recent studies performed by our group on the relationship between loosely bound water and organic volume made possible to calculate an approximation of α_2 from experimental mineral and organic volumes. Those data were available in all NEC lesions of this study, and our approximate experimental α_2 was given by [22]:

$$\alpha_2^{\exp} = \alpha_2^{theo} - 0.5759 - 0.7396\Delta\beta \quad (2)$$

α_2^{theo} is the predicted α_2 as a function of the experimental mineral volume and its volume *fraction* is calculated by [11]:

$$\alpha_2^{theo} = 0.6987 - 1.2487 \cdot \left(\frac{V_1}{100}\right) + 0.544 \cdot \left(\frac{V_1}{100}\right)^2 \quad (3)$$

And $\Delta\beta$ is the difference between experimental and predicted organic volume. The fraction of the predicted organic volume is given by [11]:

$$\beta_{theo} = 0.08654 + 0.46808 \cdot \left(\frac{V_1}{100}\right) - 0.584 \cdot \left(\frac{V_1}{100}\right)^2 \quad (4)$$

The results of Eqs. (3-4) have to be multiplied by 100 so that they can be inserted in Eq. (2). α_2^{theo} is a parameter inversely related to pore viscosity.

Thus, we assumed that dried NEC had an air volume equal to $\alpha_2^{\exp}$. By the use of this value in the mathematical approach for interpretation of BR_{obs} by Sousa et al [20], it could be possible to quantify the volumes infiltrated by quinoline (α_2^{qui}), by air (α_2^{air}) (if any) and α_1, reasonably approaching to the real situation.

2.5 Real-time two-dimensional mapping of the infiltration of quinoline

Thirteen out of the twenty samples were selected to perform real-time mapping of quinoline infiltration into NEC. As described in [16], an orientation-independent polarizing microscope system with one variable retarder (known as "single polscope") [23] was used to map two-dimensional changes in birefringence during infiltration of dried enamel by quinoline. This system obtains the phase retardance values at all points of the sample in the field of view independently of the sample orientation, by rotating the polarization states of light rather than rotating the sample, making it possible to explore new information on the transport of materials in enamel. Along the light path of the transmitted light microscope, the main components of the system consisted of an interference green filter (546 nm, bandwidth of 10 nm, Edmund Optics, USA), a rotatable linear polarizer, a liquid crystal variable retarder covered with an achromatic quarter-wave retardation film for 544 nm (Meadowlark, USA), the sample (between glass slide and cover glass and immersed in test liquid), a 4X pol fluorite objective lens, a second achromatic quarter-wave retardation film for 545 nm (Meadowlark, USA), a second linear polarizer, and a digital camera in monochromatic mode (Nikon D7000, Nikon, Japan). Both quarter wave-films were aligned at +45º. The liquid crystal generates different polarization states of light when voltage is applied. The four-frame algorithm that employs four polarization states in response to four specific applied voltages was applied [23]. Each polarization state was obtained by the following sequence of azimuths of the optic axes of the liquid crystal: 270º, 225º, 180º, and 135º. The voltages used to generate such azimuths were provided by the manufacturer of the liquid crystal. Voltages were applied by a signal generator (model AFG 3021B, Tektronix, USA) using AC voltage with square wave and frequency of 2 kHz. The Single Polscope is able to quantify retardances up to $\lambda/2$ for maximum angle of 90º of the first polarizer. An angle of 87º was used,

which allowed measurements of retardances up to 265 nm. The system was calibrated with a sample of normal enamel with points where retardance had been measured manually with the Berek compensator. A good agreement between the two systems was found.

After drying, the sample was placed between a glass slide and a cover glass and quinoline was injected with a brush into the space between cover glass and glass slide and diffused to the sample. Starting one minute after the injection of quinoline, a series of measurements of changes in birefringence were performed in the following time intervals: at 1 minute intervals within the first 10 minutes, at 5 minutes intervals up to 1 hour after injection. In two samples changes were registered for a longer time, using the following time intervals: at 3 minute intervals up to 30 minutes after immersion in quinoline, 10 minutes intervals up to 70 minutes after immersion in quinoline, at 30 minutes intervals up to 3.5 hs after immersion in quinoline, at 1 hour intervals up to 9.5 hs after immersion in quinoline, and at 12, 36 and 48 hs after immersion in quinoline.

Technical problems did not allow registration of longer periods for all samples. During each series, both the digital camera and the signal generator were controlled by customized software that automatically synchronized the signal generator (to release the proper voltage to the liquid crystal) and the digital camera (to shoot). The four resulting images were treated with the four-frame algorithm provided by Shribak [23], resulting in an image of the map of birefringence in enamel. Changes in retardance (retardance multiplied by sample thickness is the birefringence) were used to map the infiltration of the liquids.

2.6 Data analysis

The relationship between the proportion of the pore volume infiltrated by quinoline and the major volume component (mineral volume, α, β, and α_d,) were calculated. To test our

hypothesis, differences between particular R^2 parameters were tested using Cohen's effect size for proportions [24]:

$$h = \phi_x - \phi_y \qquad (5)$$

and

$$\phi = 2 \cdot \arcsin \sqrt{P} \qquad (6)$$

In Eq (6) P is the R^2 coefficient of a given parameter. When testing predictors of the proportion of the pore volume infiltrated by quinoline (α_2^{qui}/V_2) ϕ_x and ϕ_y were related to R^2 coefficients of α_d and of another parameter (mineral volume, α or β) under comparison, respectively. For other comparisons, ϕ_x and ϕ_y were related to the higher and the lower R^2 parameters being compared, respectively. Real-time 2D-mapping of quinoline infiltration was analyzed qualitatively by visually examining videos made with the acquired birefringence images.

3 Results

Real-time 2D-mapping of infiltration is shown in Video 1, revealing that the first stages in retardance changes, represented by a wave coming from the innermost enamel towards the outer enamel and following the prisms paths. The displacement of material (probably water) represented by such wave filled the body of the lesion from the bottom to the surface layer, also following prisms paths. After that, a new wave appeared, at this time coming from the original

enamel surface inward, following the prisms paths, but with a lower rate this time. This inward wave (probably representing infiltration of quinoline) occurred only at a restricted area: the one where the body of the lesion had the deepest depth into the enamel layer. Changes in the remaining parts of the enamel layer were negligible up to 1 hour.

In one of the lesions, the 2D-mapping of the infiltration was registered up to 48 hours and more details related to the late stages than to the early stages were registered. An inward penetration, starting at the original enamel surface, following prism paths towards the bottom of the body of the lesion, was registered (Video 2). At some time during this infiltration, some regions in the body of the lesion (the center of the field of view, just below the surface layer) underwent a reduction in retardance (corresponding to the dark zone) while the infiltrating material (probably quinoline) penetrated further at deeper areas of the body of the lesion. The amount of the infiltrated material at the surface layer remained unchanged while the amount located at an area just beneath it (along prisms paths) showed reduction as the material infiltrated to deeper parts. Adjacent to the area where the changes described above took place, at the left lower side (where the surface layer and part of the body of the lesion were lost), quinoline infiltrated towards the bottom of the body of the lesion decreasing the size of a dark zone under formation and penetrating a zone more internally located (translucent zone). Video 3 shows the same features shown in Video 2, but with a wider field of view.

Fig.1 shows typical histological features of NEC lesions (located in mid-crown enamel) under all immersion media used and the path containing the histological points where quantitative measurements were performed. In water, a positively birefringent (positive BR_{obs}^{water}) body of the lesion is surrounded by two negatively birefringent zones (negative BR_{obs}^{water}), the surface layer and the inner enamel, respectively (Fig. 1A). In air, the positive body of the lesion with positive BR_{obs}^{water} and part of the surface layer became opaque (no birefringence), and inner

enamel had parts with both positive BR_{obs}^{water} and negative BR_{obs}^{water} (Fig. 2B). Without the Red I filter, opaque enamel has the same color of the background (Fig. 2C). In quinoline, most of the surface layer and the whole body of the lesion with positive BR_{obs}^{water} became translucent (Fig. 1D). A translucent zone is located between the isotropic dark zone and isotropic inner enamel (Fig. 1D), and this later is slightly increased in relation to the size of the isotropic zone in inner enamel under air immersion (Fig.1B). The outer part of the NEC lesion is shown radiolucent under microradiography (Fig. 1E). In pseudo-colors, the microradiograph shows that the outer 300 μm of dentin is also demineralized (Fig. 3F).

Component volumes were measured at 1124 histological points from all lesions. Data on the component volumes measured along the line shown in Fig 1 revealed that mineral volumes were lower than 80% (Fig. 2A). Regarding non-mineral volumes, water volume profile had "U" shaped curve with the highest values in the positively (in water) body of the lesion (Fig. 2B), while organic volume had a decreasing profile from the enamel surface inward (Fig. 2C). The volume infiltrated by quinoline and α_d had very similar profiles up to ~500 μm from the enamel surface, and thereafter α_d remained relatively flat while α_2^{qui} decreased until reaching zero at ~700 μm from the enamel surface (Fig. 2D). The outer part of the enamel layer (which includes the surface layer, body of the lesion with positive BR_{obs}^{water}, dark zone and translucent zone) had some parts of its pore volume infiltrated by quinoline (Fig. 2D). After immersion in quinoline, some air remained in the pores and this air volume showed an increasing profile from the middle of the body of the lesions inward up to approximately reaching a plateau in inner enamel (Fig. 2E). The firmly bound water remaining after quinoline immersion showed a roughly flat profile with values ranging from 7 to 10% (Fig. 2F).

In our sample, the translucent zone was found in 13 lesions, and in 10 of them the enamel more internally located had mineral volumes lower than expected for normal enamel (i.e. < 88%).

The dark zone was found in all lesions, presenting either a small part located in the body of the lesion with positive BR_{obs}^{water} (11 lesions) or entirely located in the inner enamel with negative BR_{obs}^{water} (9 lesions). In one lesion (without positive BR_{obs}^{water}) no dark and translucent zones were not seen and quinoline did not infiltrate (data not shown). In the lesion shown in Fig.1, the translucent zone was not the lesion front and the dark zone was entirely outside the body of the lesion with positive BR_{obs}^{water}. The lesion shown in Fig. 3 (see arrow) is an example of a dark zone partially located in the body of the lesion with positive BR_{obs}^{water} and opacity under air immersion.

From all major component volumes, α_d was shown as the best predictor of the proportion of pore volume infiltrated by quinoline (α_2^{qui}/V_2) (Fig. 4), predicting 60% of variances (Fig. 4D). The effect sizes of the differences were: 1.572 for α_d x V_1; 0.677 for α_d x α; and 0.974 for α_d x β. Comparing α_d values of quinoline with the one of Thoulet's solution with refractive index 1.47 [16], the effect size was 0.19.

In the outer part of the enamel layer, the distance from the enamel surface showed moderate inverse relationships with both α_2^{qui}/V_2 (R^2 = 0.155; Fig. 5A) and α_2^{qui} (R^2 = 0.248; Fig. 5B). Considering the flow mechanics during infiltration of quinoline, we tested the hypothesys that α_d would be directly related to the negative BR_{obs}^{water}. In the outer part of the enamel layer, a very strong direct relationship (R^2 = 0.798) was found between those parameters, but in the inner part a lower R^2 (0.424) was found. The effect size of the differences between these R^2 values was 0.791. Effect sizes are classified as [24]: negligible (0-0.2); small (< 0.5); medium (0.5< ES < 0.8); and large (≥ 0.8).

4 Discussion

Combining information on component volumes, permeability (α_d) and flow mechanics (real-time 2D-mapping), our data provide completely new information on changes in NEC during infiltration of an oil medium. In this report we focused on the pattern of infiltration, whilst more in depth details of both dark and translucent zones will be reported in a future publication. Confirming a recent report on NEC, most of the transport processes took place along prisms paths and were restricted to the main body of the ground sections. The first evidence that transport of materials occurs mostly along prisms paths in ground sections of enamel was shown by Medeiros et al [15] with water displacement in normal enamel. Data on the flow mechanics of the first stages following immersion in quinoline provided evidences suggesting a water flow from inner to outer enamel, following prisms paths, filling the body of the lesion (that part with positive BR_{obs}^{water}) from the bottom up. The reasons why the material in this early flow is considered as water are: (i) quinoline has been shown to cause dehydration in ground sections of NEC [25]; (ii) a considerable amount of firmly bound water remained, after drying, in the inner part of the enamel layer of our samples (Fig. 2F); (iii) the flow rate was relatively fast; and (iv) considering prism paths as the main pathways, the outward flow occurred towards the location with the higher concentration of quinoline.

The fact that water flowed following prisms paths is even more remarkable than the recent report that Thoulet's solutions also do so. Because water is less viscous than Thoulet's solution and is the main component in both prisms' sheaths and prismatic and inter-prismatic enamel [9], it was expected that the osmotic pressure caused by quinoline at the entrance of the prism's paths at the original enamel surface would cause random movement of water. The observed water flow is astonishingly, indicating that the most of the loosely bound water in NEC is located in prisms sheaths. Probably, the higher negative capillary pressure found in the smaller

nanopores [26] is the main force responsible for a more firmly bound water in prismatic and inter-prismatic pores. As highlited recently [16], this suggest that demineralization mostly results in growth of the major pores in prisms' sheaths and those pores enlarge at the expenses of the intra-prismatic enamel. Otherwise, neighboring prisms' sheaths would connect each other laterally, causing random diffusion of water during the early stages after immersion in quinoline. We recognize, however, that this needs further structural confirmation. Nevertheless, it can be said that the enamel structure is highly preserved in NEC, confirming recent nanostructural characterization with high resolution 3D X-ray scattering [8]. This water flow is evidence that flow in the opposite directions is expected when aqueous liquids (that do no cause dehydration) are infiltrated into dry NEC. This has important implications for remineralizing agents that are very fluid. They might be transported to inner enamel by that flow along prisms sheaths, decreasing remineralization in the main body of the NEC lesion. Analysis of flow mechanics of the infiltration of remineralizing agents might be able to help in the development of agents with improved remineralization efficiency.

The key assumption in classic enamel studies that quinoline is the first material penetrating into enamel pores in dried ground sections of NEC [5, 6, 14] is inconsistent, compared to the data presented by this study. During the initial stage, because quinoline is a dehydrating agent [25], there occurs an outward water flow exerting a force against penetration of quinoline, which comes after the water flow is ceased. Then, quinoline flows starting at the original enamel surface following prisms' paths towards the bottom of the body of the lesion. As the flow proceeds, α_d is the main factor determining the pore volume occupied by quinoline (α_2^{qui}/V_2) (Fig.4D). This later is gradually reduced with the distance from the enamel surface until reaching zero where the permeability of the forthcoming points are reduced to a certain value (Fig. 2D). Before infiltration is completed, both the dark and translucent zones are infiltrated by quinoline (Video 2). Our results show that quinoline hardly filled more than 50% of the pore volume,

indicating that there was enough water (as α_1), although in a more viscous pore compartment, available for further diffusion of other agents after infiltration in quinoline. The permeability of the remaining pore volume is lower because α_1 is lower than the total water volume. This parameter of permeability is expected to be the main factor controlling diffusion of other agents (eg. acid solutions) in infiltrated enamel. We propose that resin infiltrants should be tested based on the reduction of permeability they cause after infiltration.

Confirming our hypothesis, prediction of the infiltration of quinoline by α_d was improved compared to Thoulet's 1.40 and 1.47, in spite of a low effect size (0.19). It was also confirmed that distance from enamel surface is a factor reducing the infiltration of quinoline (Fig. 4A-B). The implication of the effect sizes of differences in predictions on the proportion of pore volume infiltrated by different materials needs to be investigated.

Most of the body of the lesion and the surface layer became opaque after drying (Fig. 1C-D; Fig 3C-D). The birefringence related to the pore material is the form birefringence, produced by materials (not intrinsically birefringent, but with different refractive indexes) with dimensions that are small in relation to the wavelength of light used (546 nm in this study) [27]. Most probably, sizes of pores filled with air at those zones exceeded the threshold of small compared to the wavelength (which is ~20% of 546 nm = 110 nm), resulting in the lack of birefringence. This explanation is consistent with recent report of pores sizes up to 200 nm in the body of the lesion [8]. Some parts of the dark zones were located inside the opaque area seen under air immersion (at the body of the lesion with positive BR_{obs}^{water}) (Fig. 3), in agreement with previous reports [4], contradicting the predominant interpretation that the dark zone is a universal feature of an area with reduced pores sizes and that they probably resulted from remineralization [5, 6, 7]. In addition, we showed that both the dark and the translucent zones were infiltrated by quinoline. On this basis, histological features of NE in quinoline are not a matter of infiltrated (large pores) or not-infiltrated (small pores), but rather are a result of the combined effect of permeability,

distance from enamel surface (the starting point of penetration), effective pore size (α) and time (Fig. 4 and Videos 2 and 3). The histopathological features shown here describe NEC lesions as a result of loss of mineral volume and gain of both water and organic volumes.

Our results are consistent with the reduction of the dark zone after removal of organic matter [12], what can be explained by the fact that removal of organic matter is expected to increase permeability (α_d).

The strong relationship between BR_{obs}^{water} and α_d in the outer part of the enamel layer indicates that permeability of NEC lesions in ground sections can be fast screened based on the qualitative distribution of BR_{obs}^{water}. Once prisms' paths are the main pathways for transport of materials in intact teeth [28], and recent data indicate that this is the same in ground sections of NEC [16], fast screening of NEC ground sections combined with real-time 2D mapping might provide an invaluable technique for exploring flow mechanics of both remineralizing and infiltrant agents, opening new avenues for enhancing non-invasive treatment of NEC lesions. The less strong relationship between BR_{obs}^{water} and α_d in the inner part of the enamel layer gives further evidence of the important of 2D mapping in diffusion in NEC.

In conclusion, we confirmed our hypothesis that an improved prediction of material infiltration in NEC lesions by α_d was achieved with quinoline and that distance from the original enamel surface is a factor for reducing the infiltration of quinoline, which, when NEC are immersed in, resulted in an early outward water flow followed by a late inward flow of quinoline, both following prisms paths in the main body of ground sections. Data on flow mechanics, spatially-resolved quantification of component volumes and birefringence opened new avenues for exploring diffusion of remineralizing agents and resin infiltrants in ground sections of NEC lesions.

Acknowledgements

The authors would like to express their sincere thank to Dr Michael Shribak (Marine Biological Laboratory, USA), who helped with the selection of the appropriate parts of the single polscope and their alignment in single polscope setup, and Mr. Yuri Gonzaga (Master in Computer Science, Federal University of Paraiba, Brazil), who developed the softwares used to control the single polscope and obtain retardance images. The first two authors of this study were financially support by scholarships from CNPq (Brazilian Ministry of Science, Technology and Innovation).

Disclosures

Authors declare that there are no conflicts of interests.

References

[1] Williams JL. A contribution to the study of pathological enamel. Dent Cosmos 1987; 39, 169, 269, 353, 413.

[2] Applebaum E. Incipient dental caries. J Dent Res 1932; 12: 619.

[3] Darling AI. Studies of the early lesion of enamel caries of transmitted light, polarised light and radiography. . Br Dent J 1956; 101: 289-297.

[4] Darling AI. Studies of the early lesion of enamel caries. Br. Dent. J 1958; 105: 119–135.

[5] Poole DGF, Mortimer KV, Darling Al, Ollis WD (1961). Molecular sieve behaviour of dental enamel. Nature 1961; 189: 998-1000.

[6] Darling AI . The selective attack of caries on the dental enamel. Ann. R. Coll. Surg. Engl. 1961; 29: 354–369.

[7] Robinson C, Shore RC, Brookes SW, Strafford S, Wood SR, Kirkham J. The chemistry of enamel caries. Crit. Rev. Oral. Biol.Med. 2000; 11: 481–495.

[8] Deyhle H, White SN, Bunk O, Beckmann F, Müller B. Nanostructure of the carious tooth enamel lesion. Acta Biomater 2014; 10: 355-364.

[9] Shellis RP, Dibdin GH: Enamel microporosity and its functional implications; In: Teaford MF, Smith MM, Ferguson MWJ (eds): Development, Function and Evolution of Teeth. New York, Cambridge University Press, 2000, 242–251.

[10]Houwink B. The limited usefulness of Thoulet's solution in imbibitions experiment in dental enamel. Br Dent J 1969; 126: 447-450.

[11] Sousa FB, Vianna SS, Santos-Magalhães NS. Dental enamel birefringence for a wide mineral content range and for different immersion media's refractive indexes: an improved mathematical interpretation. J Microsc 2009; 23: 69-75.

[12] Shellis RP, Hallsworth AS, Kirkham J, Robinson C. Organic material and the optical properties of the dark zone in caries lesions of enamel. Eur. J. Oral Sci 2002; 110: 392–395.

[13] Crabb HSM. Enamel caries: observations on the histology and pattern of progress of the approximal lesion. Br Dent J 1966; 121: 115 Pt 1: 161 Pt 2.

[14] Hallsworth, A.S., Robinson, C. & Weatherell, J.A. (1972) Mineral and magnesium distribution within the approximal carious lesion of dental enamel. Caries Res. 6, 156–168.

[15] Medeiros RCG, Soares JD, Sousa FB. Natural enamel caries in polarized light microscopy: differences in histopathological features derived from a qualitative versus

a quantitative approach to interpret enamel birefringence. Journal of Microscopy 2012; 246(2): 177-189.

[16] Meira K, Brito C, Sousa FB. Natural enamel caries: predicting permeability of the surface layer. Acta Biomater 2014 (Submitted).

[17] Ismail AI, Sohn W, Tellez M, Amaya A, Sen A, Hasson H et al. The International Caries Detection and Assessment System (ICDAS): an integrated system for measuring dental caries. Community Dent Oral Epidemiol 2007;35:170–8.

[18] Angmar B, Carlstrom D, Glas JE . Studies onthe ultrastructure of dental enamel. IV. The mineralization of normal human enamel. J. Ultrastruct 1963; 8: 12-23.

[19] Elliott JC. Structure, crystal chemistry and density of enamel apatites. In: Chadwick D, Cardew G (eds). Dental enamel, Ciba Foundation Symposium 205. Chichester; Wiley; 1997. pp. 54–72.

[20] Sousa FB, Vianna SS, Santos-Magalhães NS. A new approach for improving the birefringence analysis of dental enamel mineral content from polarizing microscopy. J Microsc. 2006; 221: 79-83

[21] Barbosa de Sousa F, Dias Soares J, Sampaio Viana S. Natural Enamel Caries: A Comparative Histological Study on Biochemical Volumes. Caries Res. 2013; 47:183–192.

[22] Macena MS, Leite MLA, Gouveia CL, DE Lima TAS, Athayde PA, Sousa FB. A comparative study on component volumes from outer to inner dental enamel in relation to enamel tufts. Arch Oral Biol 2014 (Submitted).

[23] Shirbak M. Complete polarization state generator with one variable retarder and its application for fast and sensitive measuring of two dimensional birefringence distribution. J Opt Soc Am A 2011; 28: 410-419.

[24] Cohen J: A power primer. Psychol Bull. 1992; 112: 155–159 .

[25] Gwinnett AJ. The pH of Thoulet's solution for various dilutions with saturated potassium iodide, Arch Oral. Biol 1965; 10:187-88.

[26] Tas NR, Mela P, Kramer T, Berenschot JW, Van Den Berg A. Capillarity induced negative pressure of water plugs in nanochannels. Nano Lett 2003; 3: 1537–1540.

[27] Stokes AR. The Theory of the Optical Properties of Inhomogeneous Materials. SPON 1963, London.

[28] Shellis RP. Transport processes in enamel and dentine. In: Addy M, Embery G, Edgar WM, Orchardson R, eds. Tooth wear and sensivity. London: Martin Duniz, 2000; 19–24.

Captions for figures and videos

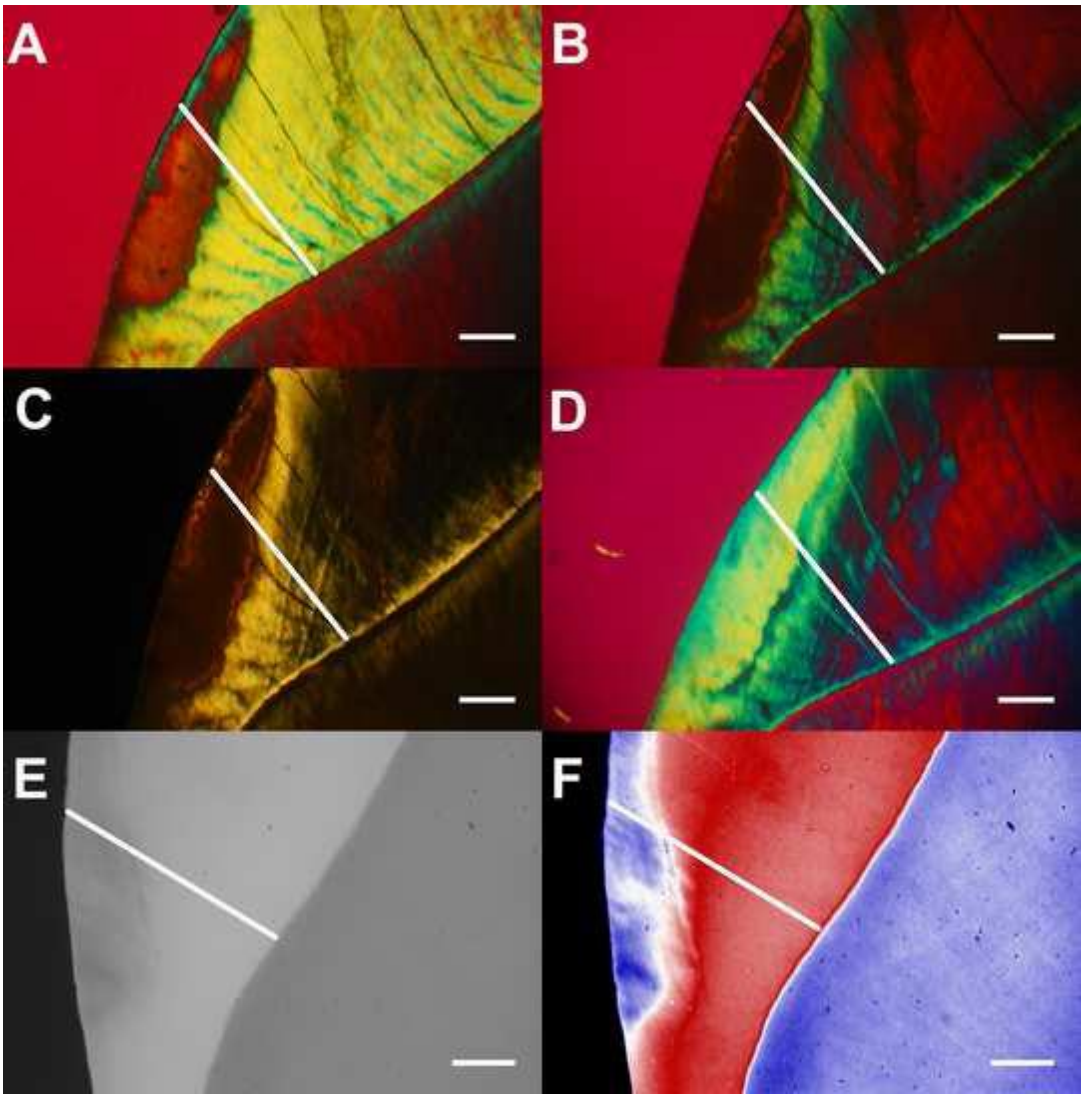

Fig. 1. Typical features of a NEC lesion in all media with the transversal line where histological points were located. A, in water, a positively birefringent (positive BR_{obs}^{water}) body of the lesion is surrounded by two negatively birefringent zones (negative BR_{obs}^{water}), the surface layer and the inner enamel, respectively. B, in air with Red I filter (red background), the positive body of the lesion with positive BR_{obs}^{water} and part of the surface layer became opaque (no birefringence), and inner enamel had parts with both positive BR_{obs}^{water} and negative BR_{obs}^{water}. C, in air but without Red I filter, opaque enamel has the same color of the background. D, in quinoline most of the surface layer, the whole body of the lesion with positive BR_{obs}^{water} became translucent, and a translucent

zone is also located between the isotropic dark zone and isotropic inner enamel. E, microradiography shows radiolucency in the outer part of the NEC lesion. F, microradiography in pseudo-colors, evidence of demineralization in the outer 300 μm of dentin adjacent to the lesion. Scale bars = 300 μm.

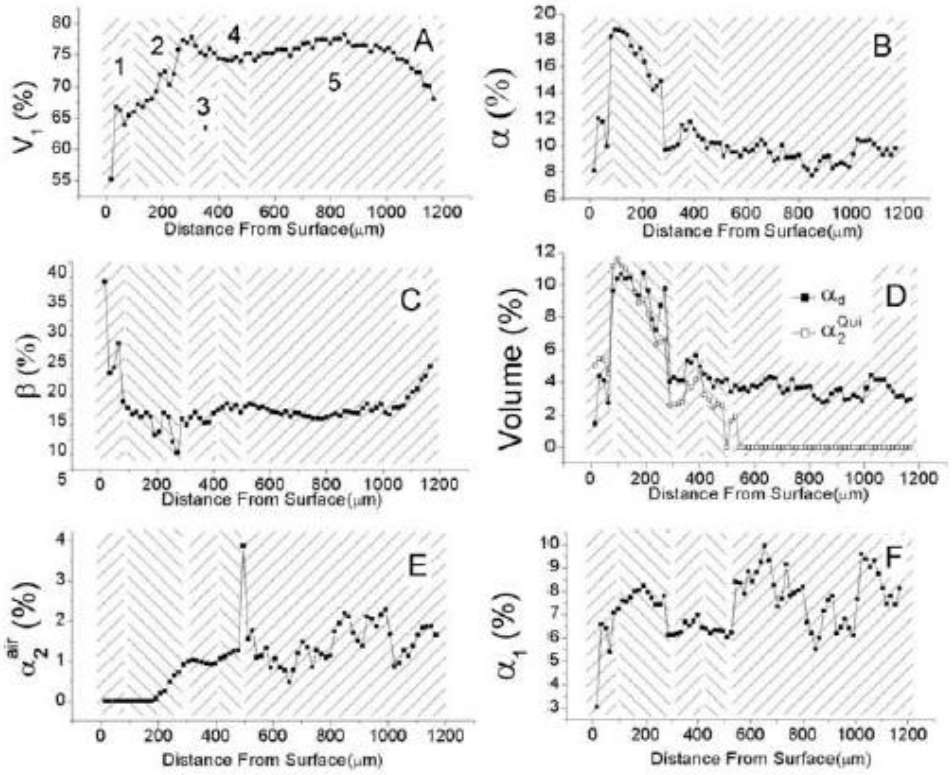

Fig. 2. Plots of quantitative component volumes found along the transversal shown in Fig. 1, distributed at the surface layer (1), body of the lesion with positive BR_{obs}^{water} (2), dark zone (3), translucent zone (4) and the inner part of the enamel layer (5). Mineral (V_1) (A), total water (B), organic (C), permeability (α_d) and volume infiltrated by quinoline (α_2^{qui}) (D), volume filled by air (α_2^{air}) (E) and firmly bound water volume (α_1) (F).

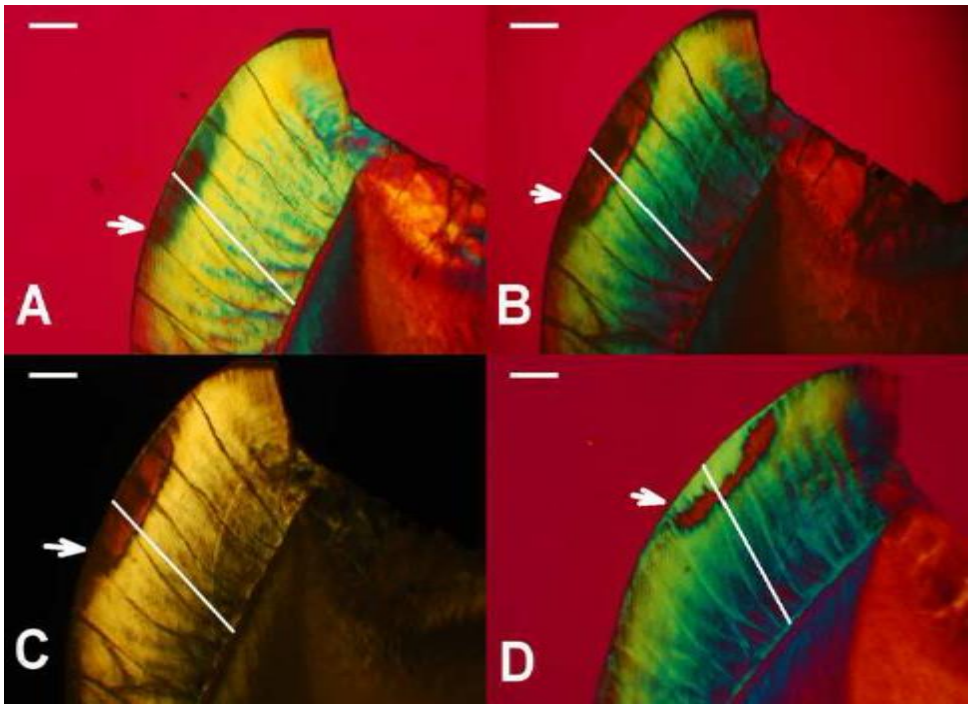

Fig. 3. Histological features under polarizing microscopy of a NEC lesion where part of the dark zone was located in the body of the lesion with positive BR_{obs}^{water}. Arrows indicate the site corresponding to the location of this part of dark zone in all media (A, water; B and C, air; and D quinoline).

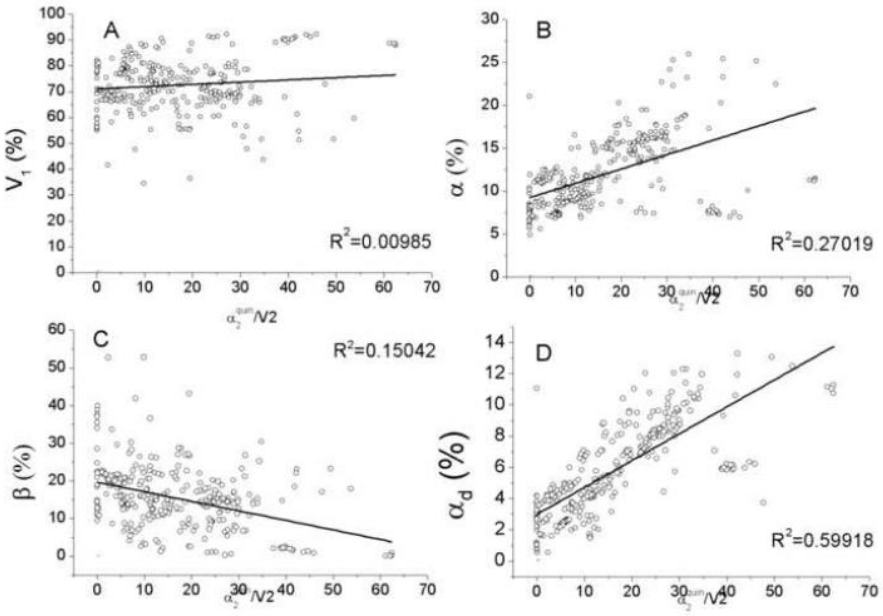

Fig. 4. Correlations between candidate predictors (A, mineral volume; B, total water volume; C, organic volume; and D, α_d) and the proportion of the pore volume infiltrated by quinoline (α_2^{qui}/V_2).

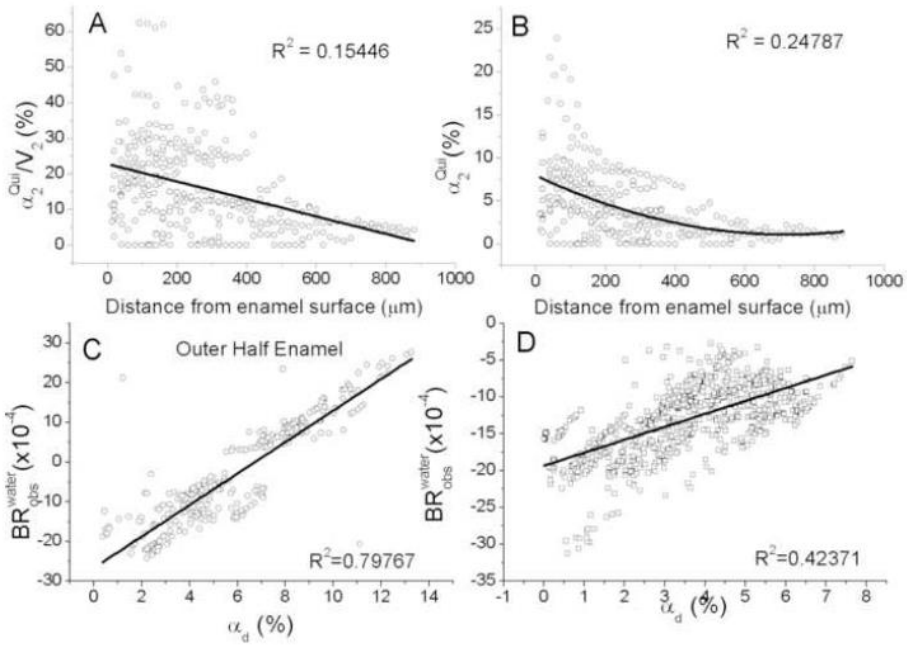

Fig. 5. A, plot of the proportion of the pore volume infiltrated by quinoline (α_2^{qui}/V_2) and the distance from the enamel surface showing a weak linear inverse correlation. B, plot of the volume infiltrated by quinoline (α_2^{qui}) and the distance from enamel surface showing a medium non-linear (2-order polynomial) inverse correlation. C, permeability (α_d) and negative BR_{obs}^{water} are shown to be strongly correlated in the outer part of the enamel layer (n = 317 histological points), while in the inner part (n = 807 histological points) the correlation is lower (D).

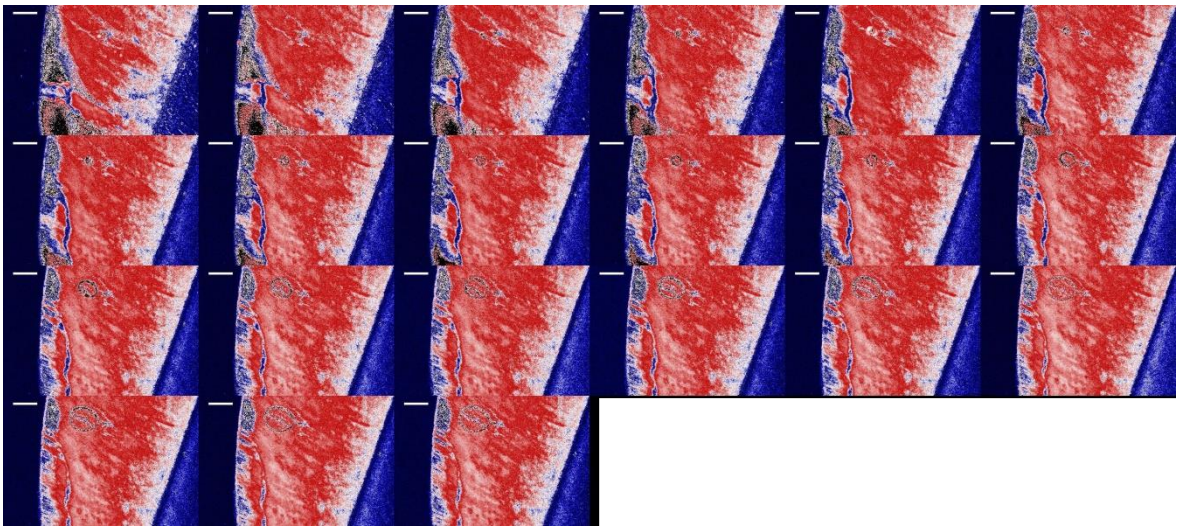

Video 1. Real-time 2D mapping (for 1 hour; 21 frames) of the infiltration of quinoline in a NEC lesion. Time interval was of 1 minute between first 11 frames, and 5 minutes between the last 10 ones. The first stages of transport processes after immersion in quinoline are shown. A wave, following prisms paths, comes from the innermost enamel towards outer enamel. The displacement of water fills the body of the lesion from the bottom to the surface layer, also following prisms paths. After that, a new wave appeared, at this time (quinoline) coming from the original enamel surface inward, following prisms paths, but with a lower rate. Infiltration of quinoline occurred only in the area with the highest depth of body of the lesion with positive BR_{obs}^{water}. After the first wave, changes in the remaining parts of the enamel layer were negligible up to 1 hour. Scale bar = 200 μm.

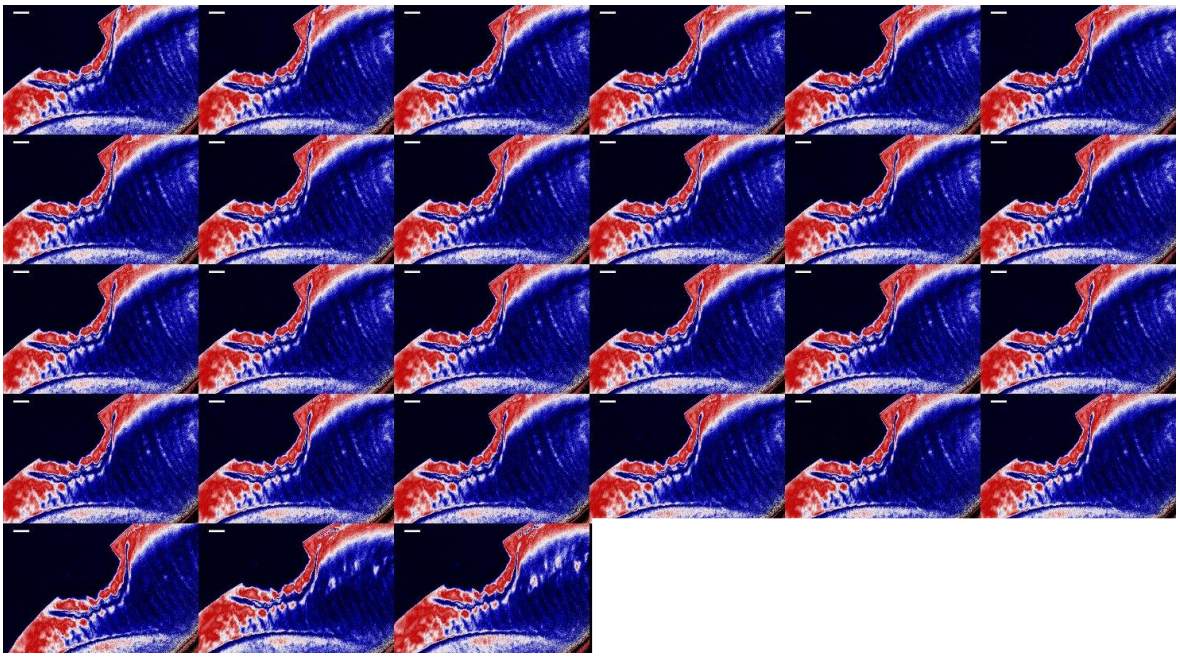

Video 2. Real-time 2D mapping of late stages of the infiltration of quinoline in a NEC lesion. The following time intervals were used: 3 minute intervals up to 30 minutes after immersion in quinoline, 10 minutes intervals up to 70 minutes after immersion in quinoline, at 30 minutes intervals up to 3.5 hs after immersion in quinoline, at 1 hour intervals up to 9.5 hs after immersion in quinoline, and at 12, 36 and 48 hs after immersion in quinoline. Quinoline penetrated from the original enamel surface (the one that already existed before cutting the tooth) following prism paths towards the bottom of the body of the lesion. At some time during this infiltration, some regions in the body of the lesion (the center of the field of view, just below the surface layer) undergone a reduction in retardance (corresponding to the dark zone) while the infiltrating material (probably quinoline) penetrated further at deeper areas of the body of the lesion. The amount of the infiltrated material at the surface layer remained unchanged while the amount located at an area just beneath it (along prisms paths) showed reduction as the material infiltrated to deeper parts. Adjacent to the area where the changes described above took place, at the left lower side (where the surface layer and part of the body of the lesion were lost), quinoline infiltrated towards the bottom of the body of the lesion decreasing the size of a dark zone under formation and penetrating a zone more internally located (translucent zone). Scale bar = 300 μm

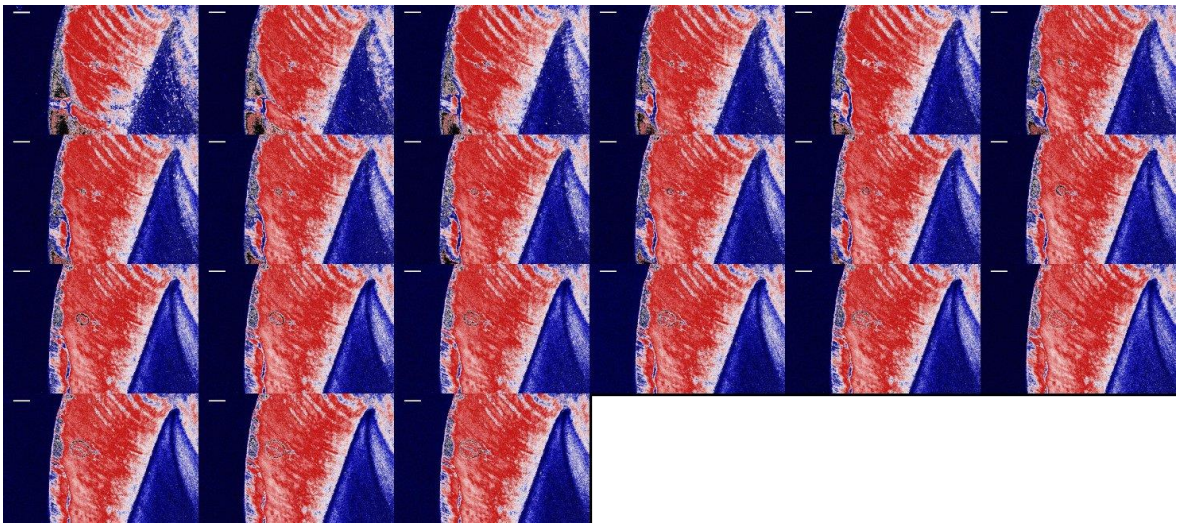

Video 3. Same event shown in video 2, but with a larger field of view. Scale bar = 200 μm.

3. CONSIDERAÇÕES GERAIS

Combinando informações sobre os volumes de componentes, permeabilidade (α_d) e mecânica dos fluidos (através do mapeamento em 2D, em tempo real), nossos dados fornecem informações nunca antes relatadas na literatura sobre alterações na lesão cariosa natural de esmalte durante a infiltração de um meio oleoso, a quinolina. Esta primeira parte do trabalho concentrou-se no padrão de infiltração, no entanto, o estudo terá continuidade e mais detalhes sobre as zonas, tanto escura quanto translúcida, serão relatados posteriormente.

4. CONCLUSÃO

Em conclusão, confirmou-se a hipótese de que uma melhor predição por α_d de material de infiltração em lesões cariosas naturais em esmalte foi obtida com quinolina, e que a distância da superfície original do esmalte é um fator para reduzir a infiltração deste meio de embebição, que difundiu como um fluxo seguindo a direção dos prismas no corpo da lesão das amostras em corte por desgaste. Dados sobre a mecânica dos fluidos, quantificação espacialmente definida dos volumes constituintes e da birrefringência, abriram novos caminhos para a exploração dos agentes remineralizantes e infiltrantes resinosos em cortes por desgaste em lesões cariosas naturais em esmalte.

REFERÊNCIAS

1. Angmar B, Carlstrom D, Glas JE . Studies onthe ultrastructure of dental enamel. IV. The mineralization of normal human enamel. J. Ultrastruct 1963; 8: 12-23.

2. Angmar-Mansson B. A polarization microscopic and micro X-ray diffraction study on the organic matrix of developing human enamel. Arch Oral Biol 1971; 16(12): 2147-156.

3. Aoba T, Moreno EC. Changes in the solubility of enamel mineral at various stages of porcine amelogenesis. Calcified Tissue International 1922; 50(3): 266-272.

4. Arends J, Ten Cate, IM. Tooth enamel remineralisation.. J Cryst Growth 1981; 53: 135-147

5. Arnold WH, Gaengler P, Kalkitschke L. Three-dimensional reconstruction of approximal subsurface caries lesions in deciduous molars. Clinical Oral Investigations 1998; 2(4): 174-179.

6. Carlström D, Glas JE, Angmar B. Studies on the ultrastructure of dental ename lV. The state of water in human enamel. J. Ultrastruct Res 1963; 8: 24-29.

7. Darling AI . The selective attack of caries on the dental enamel. Ann. R. Coll. Surg. Engl. 1961; 29: 354–369.

8. Darling AI. Studies of the early lesion of enamel caries of transmitted light, polarisad light and radiography. . Br Dent J 1956; 101: 289-297.

9. Darling AI. Studies of the early lesion of enamel caries. Br. Dent. J 1958; 105: 119–135.

10. Dibdin GH. The water in human dental enamel and its diffusional exchange measured by clearance of tritiated water from enamel slabs of varying thickness. Caries Res. 1993; 27(2): 81-86.

11. Dijkman AG, Schuthof J, Arends J. In vivo remineralization of plaque created initial enamel lesions.Caries Res 1986; 20: 202–208.

12. Driessens FCM. Physico-chemical interaction between biominerals and their environment. Ber. Bunsenges. Phys. Chem 1978; 82: 312-320.

13. Einspahr HM, Bugg CE. Esmalte, apatita e cárie: um enfoque cristalográfico. Lewis Menaker: Cáries dentárias: bases biológicas: Guanabara Koogan; 1984.

14. Ekstrand KR, Holmen L, Qvortrup K. A polarized light and scanning electron microscopic study of human fissure and lingual enamel of unerupted mandibular third molars. Caries Res 1999; 33: 41–49.

15. Elliott JC. Structure, crystal chemistry and density of enamel apatites. In: Chadwick D; Cardew G. Dental enamel. Chichester: Ciba Foundation Symposium Wiley, p.54-72, 1997.

16. Fejerskov O, Kidd E. Cárie: A doença e seu tratamento clínico, 2 ed. São Paulo: Santos; 2011.

17. Fried D, Featherstone JD, Le CQ, Fan K. Dissolution studies of bovine dental enamel surfaces modified by high-speed scanning ablation with a lambda = 9.3-microm TEA CO(2) laser. Lasers Surg. Med. 2006; 38(9): 837-45.

18. Gustafson G, Gustafson AG. Human dental enamel in polarized light and contact microradiography. Acta Odontol 1961; 19: 260–287.

19. Gwinnett AJ. Normal enamel I. Quantitative polarized light study. J. Dent. Res 1966; 45: 120–127.

20. Gwinnett AJ. Normal enamel II. Qualitative polarized light study. J. Dent. Res. 1966; 45: 261–265.

21. Hallsworth AS, Weatherell JA, Robinson C. Loss of carbonate during the first stages of enamel caries. Caries Res. 1973; 7: 345-348.

22. He LH, Swain MV . A functionally graded natural coating.Journal of Dentistry 2009; 37: 596-603.

23. He LH, Swain MV. Understanding the mechanical behavior of human enamel from its structural and compositional characteristics. J. Mech Beh of Biomed. Mater 2008; 1(1): 18-29.

24. He LH. Mechanical Behaviour Of Human Enamel And The Relationship To Its Structural And Compositional Characteristics. Sydney. Thesis. Faculty of Dentistry, Sydney University, 2008.

25. Houwink B. The limited usefulness of Thoulet's solution in imbibitions experiment in dental enamel. Br Dent J 1969; 126: 447-450.

26. Landis JR, Koch GG. The Measurement of Observer Agreement for Categorical Data. Biometrics 1977; 33(1): 159-174.

27. Medeiros RCG, Soares JD, Sousa FB. Natural enamel caries in polarized light microscopy: differences in histopathological features derived from a qualitative versus a quantitative approach to interpret enamel birefringence. Journal of Microscopy 2012; 246(2): 177-189.

28. Mellberg JR, Petrou ID, Deutchman M, Grote N. The effects of 1% pyrophosphate and 0.02% sodium fluoride on artificial caries lesion in vivo. J. Dent. Res 1988; 67: 1461-1465.

29. Nalla RK, Kinney JH, Tomsia AP, Ritchie RO. Role of alcohol in the fracture resistance of teeth. J Dent Res 2006; 85(11): 1022-1026.

30. Ogaard B, Arends J, Schuthof J, Rolla G, Ekstrand J. Action of fluorideoninitiation of early enamel caries in vivo: a microradiographic investigation. Caries Res 1986; 20: 270–277.

31. Robinson C, Shore RC, Brookes SW, Strafford S, Wood SR, Kirkham J. The chemistry of enamel caries. Crit. Rev. Oral. Biol.Med. 2000; 11: 481–495.

32. Sakae T, Suzuki K, Kozawa Y. Tooth Enamel Microstructure: A short review of studies on chemical and physical properties of enamel crystallites. . Rotterdam: Balkema; 1997.

33. Silverstone LM. Structure of Carious Enamel, Including the Early Lesion. Oral. Sci. Rev. 1973; 3: 100-160.

34. Sousa FB, Vianna SS, Santos-Magalhães NS. A new approach for improving the birefringence analysis of dental enamel mineral content from polarizing microscopy. J. Microsc. 2006; 221(2): 79-83.

35. Sousa FB, Vianna SS, Santos-Magalhães NS. Dental enamel birefringence for a wide mineral content range and for different immersion media's refractive indexes: an improved mathematical interpretation. J. Microsc. 2009; 23(1): 69-75.

36. Theuns HM, Shellis RP, Groeneveld A, Van Dijk JWE, Polle DFG. Relationships between birefringence and mineral content in artificial caries lesion of enamel. Caries Res 1993; 27: 9-14.

37. Wallace BJ. Positive birefringence in non-carious enamel. J. Dent. Res. 1961; 40: 219–219, 1961.

38. Wiener O. Die Theorie des Mischkörpers für das Feld der stationären Störung. I. Die Mittel-wertzsätze für Kraft. Polarisation und Energie. Abh. Sächs. Akad. Wiss. Math. Phys. 1912; 32: 509–604.

39. Zahradnik RT, Moreno EC. Structural features of human dental enamel as revealed by isothermal water vapour sorption. Arch. Oral Biol. 1975; 20(5-6): 317-325.